INTERNATIONAL JOURNAL FOR NUMERICAL METHODS IN FLUIDS, VOL. 10, 35–46 (1990)

NODAL INTEGRAL METHOD SOLUTIONS FOR BÉNARD NATURAL CONVECTION

GARY L. WILSON AND ROGER A. RYDIN

Department of Nuclear Engineering and Engineering Physics, School of Engineering and Applied Science, University of Virginia, Charlottesville, VA 22903, U.S.A.

SUMMARY

The nodal integral method is a relatively new numerical technique that has been used recently to solve both static and dynamic multidimensional problems in heat transfer, fluid flow and neutron transport. The method offers significant advantages in terms of stability, accuracy and efficiency over conventional finite elements when the problem can be adequately modelled in Cartesian co-ordinates. This method was used to investigate bifurcation phenomena in the Bénard problem for aspect ratios in the range of one to nine. Automatic search techniques were used with a static version to find the first four critical Rayleigh values for a square cavity, to map the first two critical Rayleigh values as a function of aspect ratio, and to examine the solution types. Accuracy enhancement was obtained by factorization and extrapolation. Critical values, obtained by interpolation, were verified dynamically. Aspect ratio crossover and transition values were found for the first two critical Rayleigh numbers, with an accuracy of the order of ± 3 per cent. The precision achieved in the results for Ra^* and Ra^{**} as a function of β is usually within 0·1%–0·2% except at high β (i.e. near $\beta = 9{\cdot}0$) and at large critical values of Ra (i.e. the first few values of Ra^{**} near $\beta = 1$). Specific results at $\beta = 1{\cdot}0$ are $Ra^* = 2584 \pm 0{\cdot}5$, $Ra^{**} = 6807$, $Ra^{3*} = 19\,734$ and $Ra^{4*} = 22\,586$.

KEY WORDS Natural convection Bénard problem Nodal integral method Bifurcation Critical Rayleigh numbers

1. INTRODUCTION

The Bénard problem is the study of the motion of a fluid in a rectangular cavity that is uniformly heated from below. This problem is of practical and theoretical importance, with applications in such diverse disciplines as engineering, meteorology and astrophysics. Of special significance, the Bénard problem provides a simple example of bifurcation in a fluid flow problem.

Bifurcation in the Bénard problem is characterized by the Rayleigh number (Ra), which is a dimensionless measure of the temperature difference across the cavity. When Ra is less than Ra^*, its first critical value, there is no fluid flow in the cavity and heat is transferred by pure conduction. When Ra is greater than Ra^*, the no-flow condition is an unstable solution and various convective cell patterns form stable solutions. As Ra is increased further, exceeding subsequent higher critical values of Ra (e.g. Ra^{**}, Ra^{3*} and Ra^{4*}), additional unstable solutions are permitted[1–3]. In general, the specific critical Rayleigh values and the specific types of solutions permitted are a function of: the aspect ratio (β), which is the ratio of length to height; the angle of cavity tilt (θ), as measured between the gravity vector and the negative y-axis; the Prandtl number (Pr); and Ra. These four non-dimensional parameters fully characterize flow in a closed cavity heated from below for a Boussinesq fluid.[4] However, Pr appears to serve primarily to scale time in two-dimensional problems.

The first reported studies of bifurcation in the Bénard problem were analytical studies of the classical infinite horizontal cavity specified in two dimensions (i.e. $\beta = \infty$). The linear theory

0271–2091/90/010035–12$06.00

Received 20 September 1988
Revised 6 February 1989

employed in these early studies led to a critical Rayleigh value of $Ra^* = 1708$ with an infinite number of convective cells (i.e. vortex rolls).[5,6] The introduction of sidewalls (i.e. $\beta < \infty$) more accurately models physical phenomena in practical engineering problems, but requires a non-linear approach owing to the resulting breakdown in the linear theory.[7] Jackson and Winters,[3] as reported by Rae,[2] used non-linear methods based on quadratic finite elements in an untilted square cavity (i.e. $\beta = 1$) to calculate the first two critical Rayleigh values. Specifically, these investigators obtained $Ra^* = 2652$ and $Ra^{**} = 7128$ using a 9×9 grid, and $Ra^* = 2612$ and $Ra^{**} = 6774$ using a 17×17 grid. Estimates of the third and fourth critical Rayleigh values were also calculated on the basis of extremely coarse grids. Using modern coarse mesh methods, Azmy and Dorning[4] calculated the first four critical Rayleigh numbers using a 6×6 mesh. The values reported were $Ra^* = 2524$, $Ra^{**} = 6807$, $Ra^{3*} = 22\,200$ and $Ra^{4*} = 23\,000$. As noted by these investigators, the critical values introduce one-, two-, three- and four-vortex solutions respectively.

The first examinations of the effects of tilt angle on bifurcation in the finite Bénard problem were conducted by Cliffe and Winters[8] and by Rae.[2] These investigators mapped the first critical Rayleigh value as a function of tilt angle, thus revealing the 'cusp catastrophe' and the limits on the tilt angle for which bifurcation of the solution takes place. Azmy and Dorning[9] mapped more fully the unfolding of the first bifurcation point and the opening of the second bifurcation point for the square cavity. These investigators failed to resolve fully the unfolding of the second bifurcation point; however, additional work on this problem has been published by Riley and Winters.[10]

The first two critical Rayleigh values in the Bénard problem, and to a much lesser extent the third and fourth critical values, have been examined by several authors as a function of aspect ratio greater than or equal to unity.[2,3,9] Azmy and Dorning also examined aspect ratios over the range $\beta = 0{\cdot}5$–$1{\cdot}0$,[9] but these results demonstrated rather uninteresting monotonic behaviour because they did not cover low enough values of β (note that the definition of aspect ratio as employed by Azmy and Dorning is the inverse of the value defined here and as used by other investigators). All investigators used relatively coarse meshes and generally restricted themselves to aspect ratios less than approximately four. This restriction on the aspect ratio means that only the first three crossovers were mapped and asymptotic regions were missed. Azmy and Dorning used a 6×6 grid (or a 4×8 grid) to investigate as many as five vortices. This process results in significant error being introduced and is probably the primary reason why their critical Rayleigh values so quickly dropped below the analytic value of $Ra^* = 1708$.

The third and fourth critical Rayleigh numbers were examined in some detail by Azmy and Dorning,[9] who also reported on a peanut-shaped vortex at $\beta = 1{\cdot}8181$. Wilson *et al.*,[11] using dynamic nodal integral methods, examined the dynamic stability of alternative solutions for $\beta > 1$ and found that unstable initial solutions will reform into stable solutions for the given values of Ra and β; they also briefly examined the existence of two separate stable solutions at critical values of the aspect ratio (i.e. crossovers).

This paper deals with the static and dynamic behaviour of convection in the Bénard problem for $1 \leqslant \beta \leqslant 9$ and $\theta = 0$. The results were extended to these higher values of β using a combination of the time-dependent nodal integral method (TDNIM)[12] and the static nodal integral method (SNIM).[13] The SNIM was derived from the TDNIM by forcing the face-average values at adjacent time steps to take on the node-integral-average value and then reducing the number of equations. Special attention was given to critical values of the aspect ratio and to the nature of solution changes at transitional values of the aspect ratio. All values for Ra^* and Ra^{**} were linearly corrected using a piecewise linear extrapolation process and continuity considerations based on extrapolated test values and test point calculations. In the region approaching $\beta = 9$, the Ra^* and Ra^{**} curves as a function of β indeed asymptotically approach the analytic value of $Ra_{crit} = 1708$.

Static nodal integral methods are very accurate and stable on a coarse mesh, while dynamic nodal integral methods are unconstrained by a Fourier or Courant conditions. Only the static method is capable of mapping allowed unstable solutions, because it will converge to such a solution when an approximate allowed solution is applied as an initial condition. Otherwise, the SNIM returns to a no-flow condition. The dynamic method, on the other hand, is used to test a solution to see how it undergoes transition to the stable state and also to generate various initial conditions. Had the objective of our study been solely to locate critical bifurcation values, then various automatic bifurcation search techniques[14] would probably have been more cost-effective. However, our goal was not only to locate these points, but also to explore the nature of the solutions and solution transitions in the vicinity of these points. A comparison of the relative efficiency of our methods against finite elements has not been done for the present problem, but such a comparison has been done for a non-linear, two-dimensional heat conduction benchmark case.[15] There the nodal integral method had a cost-accuracy efficiency advantage of about six times per spatial dimension and a clear superiority for time steps larger than the Fourier condition value.

2. PROBLEM FORMULATION

Many practical problems of interest in natural convection occur where the sole driving force for the flowfield is the bouyancy force arising from thermally induced density differences at different locations in the fluid. In such problems the flowfield is well approximated by the Boussinesq equations, where the fluid is treated as incompressible in all terms except the bouyancy terms of the momentum equations. In two-dimensional Cartesian geometry the dynamic formulation of the Boussinesq equations in dimensionless form may be written

$$\frac{\partial u}{\partial x}+\beta\frac{\partial v}{\partial y}=0 \tag{1}$$

$$\frac{\partial u}{\partial t}+u\frac{\partial u}{\partial x}+\beta v\frac{\partial u}{\partial y}+\frac{\partial \tau_x}{\partial x}-\beta\frac{\partial^2 u}{\partial y^2}-\beta\frac{Ra}{Pr}\sin(\theta)T=0, \tag{2}$$

$$\frac{\partial v}{\partial t}+u\frac{\partial v}{\partial x}+\beta v\frac{\partial v}{\partial y}+\beta\frac{\partial \tau_y}{\partial y}-\frac{1}{\beta}\frac{\partial^2 v}{\partial x^2}-\beta\frac{Ra}{Pr}\cos(\theta)T=0, \tag{3}$$

$$\frac{\partial T}{\partial t}+u\frac{\partial T}{\partial x}+\beta v\frac{\partial T}{\partial y}-\frac{1}{\beta Pr}\left(\frac{\partial^2 T}{\partial x^2}+\beta^2\frac{\partial^2 T}{\partial y^2}\right)=0, \tag{4}$$

where β (aspect ratio) and θ (tilt angle) are as defined previously, and u, v and T are the dimensionless x- and y-components of velocity and temperature respectively. Ra and Pr are the dimensionless Rayleigh number and Prandtl number, which are defined by

$$Ra=8g\alpha\Delta TH^3\rho^2C_p/\mu k, \tag{5}$$

$$Pr=\mu C_p/k, \tag{6}$$

where g, α, ρ, C_p, μ and k are the acceleration due to gravity, the coefficient of thermal expansion, density, heat capacity, viscosity and thermal conductivity respectively; ΔT is the temperature difference between the hot and cold walls; and H is the half-height of the cavity. The normal stresses τ_x and τ_y are defined by

$$\tau_x=p-\frac{1}{\beta}\frac{\partial u}{\partial x}, \tag{7}$$

$$\tau_y = p - \frac{\partial v}{\partial y}, \tag{8}$$

where p is the non-dimensional static pressure. These latter terms are introduced to accommodate decoupling of the transverse-averaged equations used to obtain the solution matrix for equations (1)–(4). In the Bénard problem the bottom wall is heated and the top wall is cooled while both sidewalls are treated as insulated. No-slip boundary conditions are applied on all four walls.

The non-linear equations for natural convection in a cavity were normally solved using the SNIM, while some solutions were also checked for stability with the TDNIM. Because the derivation of the TDNIM equations from the continuous-variable equations has been described elsewhere,[11,12] only a brief sketch of the derivation is included here.

The formalism for the TDNIM consists of five main steps, which proceed as follows.

(1) Divide the spatial system into M nodes or computational cells.
(2) Transverse-integrate the continuous-variable equations within each node over all but one of the independent variables to obtain two sets of four linear ordinary differential equations in space (one set each for the two spatial dimensions) and one set of three ordinary differential equations in time.
(3) Solve for the complete solution to the linear ordinary differential equations in terms of elementary solutions and particular integrals of the source terms. These terms can include distributed sources, transverse leakage, terms arising from the transverse-averaging process, and the non-linear advection terms. The source functions are approximated by their node-integral-average values.
(4) Derive the discrete-variable equations by imposing the continuity conditions on the primitive variables and their first spatial derivatives at node boundaries.
(5) Evaluate the integral-average value of the source terms by requiring uniqueness of the node average of each of the primitive variables, and nodal balance of mass, momentum and thermal energy.

The resulting set of algebraic equations is closed by consistently applying boundary conditions on the transverse-averaged variables that are derived from the physical boundary conditions. The final set of equations is quadratically non-linear and is solved using Newton–Raphson iterations. The resulting discrete-variable equations have the face-average values as unknowns—these are *not* the discrete-node values of finite element and finite difference methods.

Velocity flowfield plots are made directly from the solution vectors of face-average velocities by plotting velocity vectors centred at the midpoint of the node face over which the continuous variable is averaged. This method has proven to be the most satisfactory even though functional fits can be made and internal values recovered. Note that the node-integral-average values are ignored in this plotting process.

The SNIM was augmented by an automatic bifurcation search algorithm. As Figure 1 shows, in the untilted rigid rectangular cavity the velocity norm of a specific solution goes to zero for Ra less than a critical value. Therefore a search can be conducted by assuming a solution that brackets the critical Rayleigh value of interest and then halving the interval and testing the converged solution at each step. In this process the velocity norm is tested. The norm used in the algorithm was the average absolute velocity over the cavity with a 10^{-7} test for flow versus no-flow. This process is probably not the most efficient way to search for bifurcation points, but it is made feasible when combined with a coarse mesh technique like the SNIM. Several other bifurcation search techniques based on finite elements have been examined by Cliffe and Winters.[14]

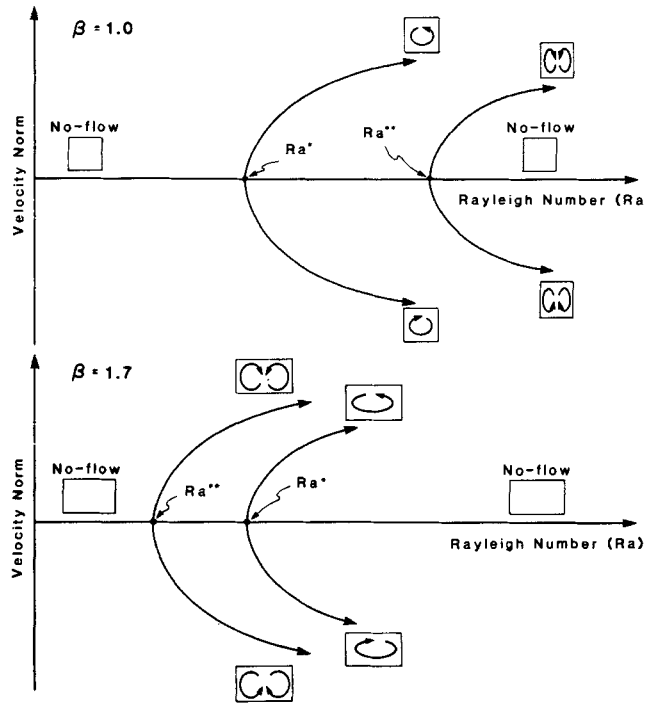

Figure 1. Schematic representation of the opening of the first two pitchfork bifurcations in the untilted Bénard problem for $\beta = 1{\cdot}0$ and $\beta = 1{\cdot}7$

3. BIFURCATION AS A FUNCTION OF ASPECT RATIO

For the case $\beta = 1$, the first bifurcation value Ra^* introduces single-vortex solutions in addition to the no-flow solution. The single-vortex solutions—the clockwise vortex and the anticlockwise vortex—are stable solutions, while the no-flow solution is unstable. The second bifurcation point Ra^{**} introduces two-vortex solutions ($\beta = 1$) that can exist in addition to the single-vortex solutions and the no-flow solution (see Figure 1). For $\beta = 1$, $Ra^{**} \gg Ra^*$ and the two vortex solutions are unstable. As β is increased, the two-vortex solutions and the single-vortex solutions change roles. As depicted in Figure 1 for $\beta = 1{\cdot}7$, $Ra^{**} < Ra^*$ and the two-vortex solutions are now the stable solutions, the single-vortex solutions being unstable.

The first two critical Rayleigh numbers have been studied by other investigators.[2,8,9] However, no one carried the process beyond the first few crossovers (to approximately $\beta = 4{\cdot}0$), and all results to date suffer from lack of accuracy.

Examinations of Ra^* using extrapolation methods of order h^n, where $n \cong 2$ or more, have verified that nodal integral methods tend to underestimate the true value of Ra^* in the region of interest. For $\beta = 1$, a best extrapolated value of $Ra^*_{best} = 2584 \pm 0{\cdot}5$ was obtained.[13] In contrast, Azmy and Dorning obtained $Ra^* = 2524$.[9] Further testing verified that nodal integral methods also lose accuracy with increasing β. Therefore, to retain high accuracy, mesh refinements are required as additional vortices are added to the permitted solutions, and the results must be compensated for increasing β. This is because accuracy is a function of the dimensional node size.

In order to obtain better estimates of the critical Rayleigh numbers and to extend the results to higher values of β, a correction function was defined so that

$$Ra = Ra_c f(\beta; h), \tag{9}$$

where Ra_c is the calculated value of a critical Rayleigh number, h is the non-dimensional (y-axis) half-node dimension and β is the aspect ratio. The correction function f was then approximated by the separable product of two functions as

$$f(\beta; h) = g(\beta)k(h), \tag{10}$$

where $k(h)$ was approximated by a constant and $g(\beta)$ was approximated by a piecewise linear function. Continuity requirements and test calculations were used in defining $g(\beta)$ when making mesh refinements. A grid size of 6×6 was employed for one-vortex and two-vortex solutions; a grid size of 12×6 was used for three-vortex and four-vortex solutions; and a grid size of 18×6 was used for five-vortex solutions and greater. A few calculations were also made with a 24×6 grid for test purposes at high values of β. Test extrapolation values were calculated on the basis of data obtained with grid sizes up to 24×24.

Figure 2 is a plot of the first two critical Rayleigh numbers as a function of aspect ratio for $\beta = 1{\cdot}0$–$9{\cdot}0$. (Calculations were made starting at $\beta = 1{\cdot}0$ and continuing with $\Delta\beta = 0.1$.) Note that these two curves define critical values of the aspect ratio (β^*) where the two curves intersect, suggesting two competing stable solutions that may be allowed, plus transition values of the aspect ratio ($\hat{\beta}$) where one solution smoothly converts into a new solution. A third class of relative minima, β_{min}—related to the preferred vortex size—can also be defined at the low point of each 'cup'.

Several characteristics of Figure 2 stand out immediately. The first critical Rayleigh value (Ra^*) maps out an 'odd-vortex' solution set, while the second critical Rayleigh value (Ra^{**}) maps out an

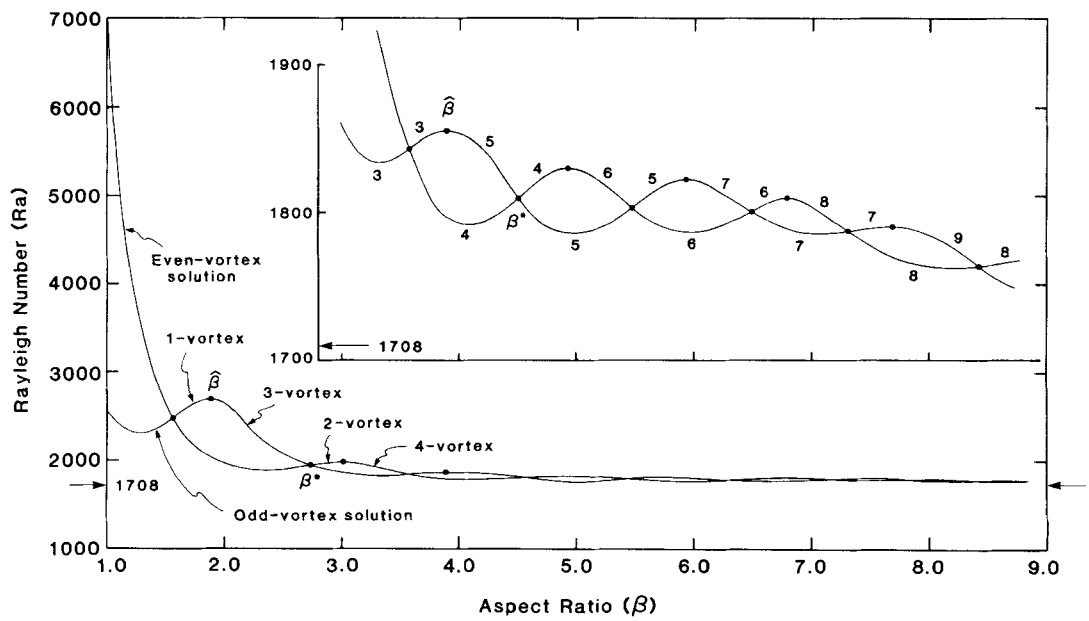

Figure 2. Ra^* and Ra^{**} as a function of increasing β

'even-vortex' solution set (i.e. a solution transition is made by adding two vortices at a time). Also note that the two curves become increasingly indistinguishable with increasing β and appear to move towards the analytic value of $Ra^* = 1708$ derived for the infinite cavity. While unproven, it is anticipated that both curves actually converge to $Ra^* = 1708$ as $\beta \to \infty$, since the relative influence of the sidewalls then becomes negligible.

The precision of the calculation of the curves presented in Figure 2 varies from at most a tenth of one per cent at low β to perhaps as much as one per cent for large β. These imprecisions result from two sources: (1) error in the calculation of the 'raw' values of Ra^* and Ra^{**} and (2) non-linear effects neglected by using a piecewise linear approximation to the correction function $f(\beta, h)$. The error resulting from the calculation of raw values is small because it is controlled. All calculations were made to within at least plus or minus one unit and then rounded to the nearest whole number. The error due to the application of the correction function cannot be as tightly controlled because of non-linear effects which become more important as the function is extrapolated out to high values of β.

4. CRITICAL ASPECT RATIOS, TRANSITION ASPECT RATIOS AND RELATIVE MINIMA

A critical aspect ratio β^* occurs at a point of intersection of the two curves formed by plotting Ra^* and Ra^{**} as a function of β. At these points, $Ra^* = Ra^{**}$ and two separate stable solutions may exist provided $Ra > Ra^*$. The fact that the number of stable solutions has indeed increased has been shown dynamically.[11]

The first eight critical aspect ratios were calculated to the nearest hundredth using interpolation techniques. These calculated values are summarized in Table I where they are compared with some recent results from Cliffe and Winters. It was originally believed that the dynamic characteristics of convection would be a strong function of the angle of intersection formed by the two curves at a critical aspect ratio; however, this does not appear to be the case. The overall accuracy of the crossover values is of the order of ± 3 per cent, and is traceable to the search technique employed.

A transition value of the aspect ratio, $\hat{\beta}$, occurs when a given solution changes to the next solution with increasing β. The transition always occurs on the upper curve with the addition of two extra vortices, going from one unstable solution form to a second unstable solution form.

Table I. Calculated values of the first eight critical aspect ratios, where Ra^* and Ra^{**} cross

Identified	Critical aspect ratio β^*		Ra^c		Number of vortices
	Present work	Ref. 16	Present	Ref. 16	
1	1·59	1·629	2485	2416	1 or 2
2	2·74	2·684	1940	1978	2 or 3
3	3·56	3·715	1843	1855	3 or 4
4	4·51		1808		4 or 5
5	5·47		1803		5 or 6
6	6·50		1799		6 or 7
7	7·31		1788		7 or 8
8	8·50		1761		8 or 9

Note: $Ra^c = Ra^* = Ra^{**}$.

Rae[2] remarked that he expected transitions to occur as β was increased as the result of intersections with the curves of higher-order solutions (e.g. Ra^{3*} and Ra^{4*}). Azmy and Dorning[9] were unable to confirm or deny this expectation. The present work and a related examination of the critical Ra^{3*} behaviour[17] do not support these early expectations. Cliffe and Winters[14] have conducted further investigations of the even and odd modes, concluding that the no-slip boundary conditions give rise to this behaviour.

In the studies of Azmy and Dorning,[9] transition values appear as relative maxima in the upper curve. However, the accuracy of their calculations dropped off rapidly with increasing β, giving increasing underestimation of the critical values, and solutions were increasingly difficult to resolve as the width of a vortex approached the width of a node. Our results for transition aspect ratios β are summarized in Table II.

As Figure 2 shows, the use of finer calculational grids and corrections for imprecisions resulting from the node size and the aspect ratio does not change the relative position of the transition values (i.e. they remain relative maxima). Transition values near $\beta = 1{\cdot}9$ (one-vortex to three-vortex solutions) and near $\beta = 2{\cdot}9$ (two-vortex to four-vortex solutions) were investigated in greater detail using 12×6 grid. Holding Ra constant at approximately its critical value, the transition value should be observable through several indicators (such as velocity norms and number of iterations). This phenomenon is illustrated in Figure 3 where the dashed line is a constant-Ra line approximately tangent to the Ra^{**} curve at its relative maxima. The velocity

Table II. Calculated values of the first seven transition aspect ratios where two vortices are added to the unstable equilibrium solution

Identified	$\hat{\beta}$	Ra^t
1	1·87	2676
2	2·875	1982
3	3·82	1857
4	4·95	1830
5	5·90	1822
6	6·86	1809
7	7·82	1788

Note: $Ra^t = Ra^*$ or Ra^{**}.

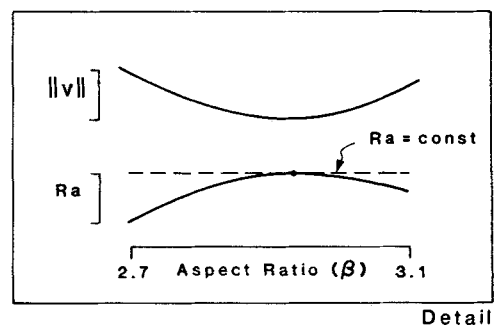

Figure 3. The velocity norm as an indicator of the transition aspect ratio

norms associated with the various solutions are plotted directly above—this curve assumes a near-zero minimum at the same location.

The initial condition for all calculations was a high-velocity, two-vortex solution. With this initial condition, the transition was examined in detail as shown in Figure 4. A peak in the number of iterations required to achieve convergence occurs at the value $\beta = 2{\cdot}875$. Normally four to eight iterations are required for convergence. This requirement grows very rapidly starting around $\beta = 2{\cdot}85$ and peaks at $\beta = 2{\cdot}875$. Surprisingly, the iteration requirements for convergence diminished almost as rapidly as they increased for further increases in β, even though the same two-vortex initial condition was used to obtain very clear four-vortex solutions. A similar peak in the number of iterations occurs using a four-vortex initial condition; however, this was not examined in as great detail. Note that transitions occur by growing two additional vortices—one at either side.

The increase in the number of iterations going from two-vortex solutions to four-vortex solutions was anticipated and was expected to be a reasonable indicator of when transition occurred. However, the occurrence of a peak rather than a threshold change was a surprise. The explanation for the peak is believed to lie in the working out of the large velocity differences between the very narrow vortices at the sides in close proximity to the strong central vortices. This is true with nodal integral methods whether the grid is sufficiently fine to actually represent these edge vortices with a plot or not.

The lower lobes in Figure 2 pass through relative minima with each successive solution. These relative minima are associated with the 'preferred size' for the particular number of vortices forming the solution, and reflect the preferred size for a single vortex at any given aspect ratio. This

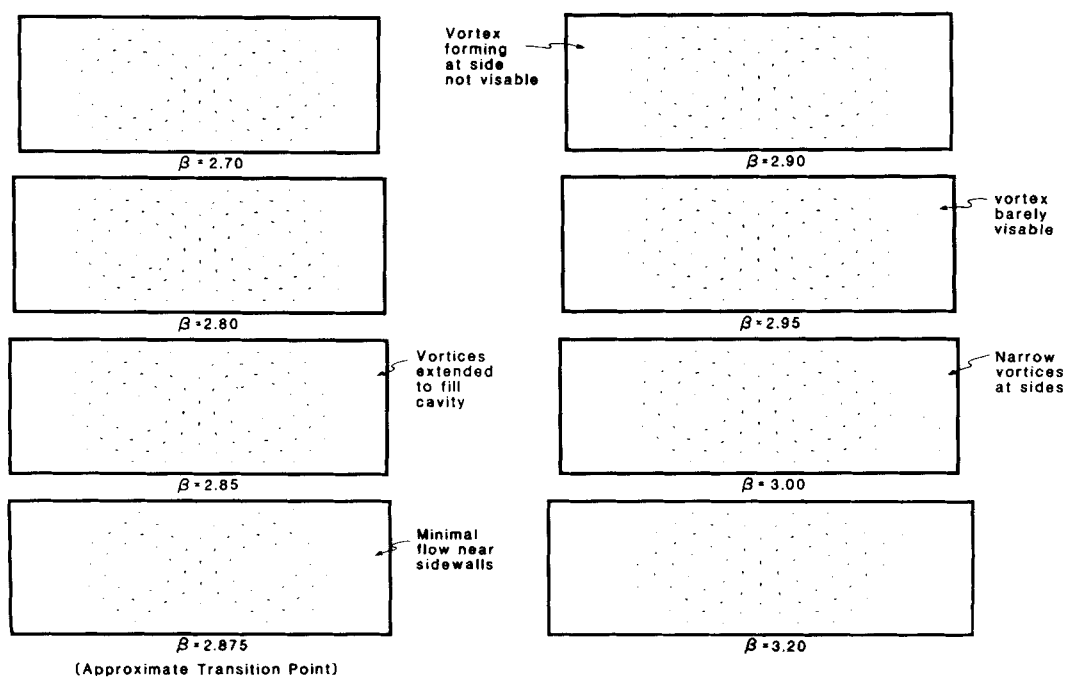

Figure 4. Flowfield development from two vortices to four vortices

Table III. Three sample calculations of the local aspect ratio

β_{min}	N	β_l
1·30	1	1·30
2·32	2	1·16
3·35	3	1·11

Note: $\beta_l = \beta_{min}/N$, where N is the number of vortices.

size can be defined by a local aspect ratio

$$\beta_l = \beta_{min}/N, \tag{11}$$

where N is the number of vortices in the solution. The analytic value of β_l for the infinitely wide cavity is $\beta_l = 1{\cdot}02$.[2]

Rae notes that the separation between minima is nearly constant at approximately 1·02 and concludes that $\beta_l = 1{\cdot}02$ at the limit; however, this result appears to be based on only two separations (i.e. the first three minima). The first three minima of Figure 2 are also separated by approximately 1·02, but the separation appears to become more variable as β increases; however, part of this variation could result from imprecisions built into the curve with increasing β.

To improve on this result, β_l was calculated using relatively fine meshes (e.g. 12×6 and 18×6 with one, two and three vortices). The process used was simply to calculate the critical Rayleigh number, varying β until the minimum was found. It was anticipated that β_l would converge towards 1·02 with increasing β. The results of these calculations are summarized in Table III for the first three minima. There is a downward trend towards 1·02, but unfortunately, the process could not be carried far enough to demonstrate convergence.

5. THE THIRD AND FOURTH CRITICAL RAYLEIGH NUMBERS

Only a few higher critical Ra have been reported in the literature. Most of the analysis has been directed at the first critical Ra^* and, to a lesser extent, the second critical Ra^{**}. However, an infinite number of bifurcation points are assumed to exist for the square cavity,[4] and estimates of Ra^{3*} (three adjacent vortices) and Ra^{4*} (four vortices arranged two-over-two) have been made. Jackson and Winters[3] obtained $Ra^{3*} = 16\,139$ using a 5×5 mesh and $Ra^{3*} = 21\,406$ using a 9×9 mesh with a quadratic finite element methodology; Azmy and Dorning[4] obtained $Ra^{3*} = 22\,200$ using a 6×6 grid with a nodal integral method. These same investigators obtained $Ra^{4*} = 41\,223$ (5×5 mesh),[3] $Ra^{4*} = 25\,032$ (9×9 mesh)[3] and $Ra^{4*} = 23\,000$ (6×6 mesh).[4] The nodal integral results of Azmy and Dorning are in fair agreement with the 9×9 results of Jackson and Winters, but all calculations suffer from the large number of vortices being represented by a very coarse mesh.

In order to refine the calculation of Ra^{3*} for $\beta = 1$, calculations were made using a 12×6 grid and a 16×8 grid (two and four times as many nodes as the grid of Azmy and Dorning). The SNIM obtained $Ra^{3*} = 19\,906$ using the 12×6 grid and $Ra^{3*} = 19\,734$ using the 16×8 grid. Doubling the number of grid points (along the x-axis) resulted in a better than 10% change from the Azmy and Dorning result of $Ra^{3*} = 22\,200$ using a 6×6 mesh, and doubling the number of nodes again resulted in less than a 1% change. Furthermore, a complete mapping of Ra^{3*} between $\beta = 1$ and $\beta = 3$ has recently been completed.[17]

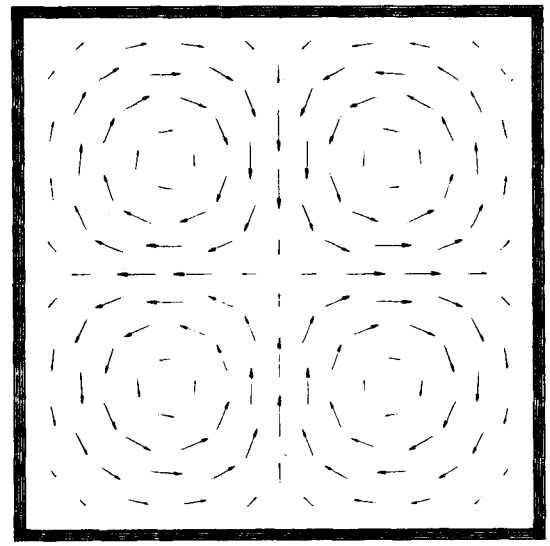

Figure 5. The four-vortex solution for a 9×9 grid with $\beta = 1$

The fourth critical Ra^{4*} introduces four-vortex solutions into the square cavity. As shown in Figure 5 for the 9×9 grid (note that nodal integral methods also accurately represent even-type solutions using odd grids), the SNIM obtained $Ra^{4*} = 22\,586$, which differs by less than 2% from the result of Azmy and Dorning.[4] This would almost seem to be in contradiction to the previous result for Ra^{3*} but it is not. The explanation lies in the symmetry of the four-vortex solution, which means that it is well modelled by the 6×6 grid. Increasing the mesh size improved the detail but did not significantly improve the solution.

6. CONCLUSIONS

The TDNIM and SNIM have been applied to the study of bifurcation phenomena in an untilted enclosed cavity for aspect ratios between one and nine. Three parameters associated with the aspect ratio (β^*, $\hat{\beta}$ and $\beta_{\min}$) were defined and evaluated. The supposition that transition values $\hat{\beta}$ appear as relative maxima was confirmed within the accuracy of the methodology; the TDNIM was used in conjunction with the SNIM to evaluate Ra^{3*} and Ra^{4*}. The new value of $Ra^{3*} = 19\,734$ was obtained as a significant improvement over the previously estimated value; however, the new value of $Ra^{4*} = 22\,586$ only confirmed previous coarse mesh results obtained with nodal integral methods. Finally, completing the Ra^* and Ra^{**} curves through $\beta = 9{\cdot}0$ at high accuracy demonstrates that the critical Ra values for the finite cavity converge towards the analytic value of $Ra = 1708$, at least to a first approximation.

ACKNOWLEDGEMENT

The authors wish to acknowledge the support given this research in the form of University of Virginia Academic Computing grants.

REFERENCES

1. F. H. Busse, *Rep. Prog. Phys.*, **41,** 1931–1967 (1978).
2. J. Rae, 'The Bénard problem revisited', *Proc. Third Int. Conf. on Numerical Methods in Thermal Problems*, Seattle, WA, 2–5 August 1983.
3. C. P. Jackson and K. H. Winters, *Int. j. numer. methods fluids*, **4,** 127–145 (1984).
4. Y. Y. Azmy and J. J. Dorning, 'Bifurcations, unfoldings and critical Rayleigh numbers in the Bénard problem', *Proc. Third Int. Conf. on Numerical Methods for Non-linear Problems*, Dubrovnik, Yugoslavia, 15–18 September 1986, 17p. Pineridge Press, Swansea, U.K.
5. Lord Rayleigh, *Phil. Mag.*, **32,** 529–547 (1916).
6. A. Pellow and R. V. Southwell, *Proc. Roy. Soc. A*, **176,** 312–343 (1940).
7. H. S. Greenside, 'Three caveats for linear stability theory: Rayleigh–Bénard convection', *Proc. Int. Conf. on Fluctuations and Sensitivity in Nonequilibrium Systems*, Austin, TX, 12–16 March 1984, Springer-Verlag, Berlin, pp. 38–49.
8. K. A. Cliffe and K. H. Winters, *J. Comput. Phys.*, **54,** 531–534 (1984).
9. Y. Y. Azmy and J. J. Dorning, 'Numerical studies of bifurcations in the confined Bénard problem', *Proc. Tenth Int. Conf. on Numerical Methods in Fluid Dynamics*, Beijing, China, 23–27 June 1986.
10. D. S. Riley and K. H. Winters, 'A bifurcation study of convection in a two-dimensional saturated porous cavity', *ASME Meeting on Bifurcation Phenomena in Thermal Processes and Convection, HTD-94 and AMD-89*, 1987, pp. 83–89.
11. G. L. Wilson, R. A. Rydin and Y. Y. Azmy, *Nucl. Sci. Eng.*, **100,** 411–425 (1988).
12. G. L. Wilson, 'Multidimensional nonlinear time-dependent nodal integral methods in heat transfer and fluid dynamics', *Ph.D. Thesis*, University of Virginia, 1987.
13. G. L. Wilson and R. A. Rydin, *Trans. Am. Nucl. Soc.*, **56,** 284–285 (1988).
14. K. A. Cliffe and K. H. Winters, *J. Comput. Phys.*, **67,** 310–326 (1986).
15. G. L. Wilson, R. A. Rydin and S. Orivuori, *Nucl. Technol.*, **82,** 94–105 (1988).
16. K. A. Cliffe and K. H. Winters, 'Numerical methods for predicting preferred and anomalous flows in Bénard convection', *Proc. Sixth Int. Conf. on Numerical Methods in Thermal Problems*, 1989.
17. G. L. Wilson and R. A. Rydin, 'Multiple equilibrium solutions to the Bénard problem at the third critical Rayleigh number', *Numer. Heat Trans. B*, **15,** 117–126 (1989).